

Condition for Break-up of Non-Wetting Fluids in Sinusoidally Constricted Capillary Channels

Igor A. Beresnev · Wenqing Li · R. Dennis Vigil

Received: 14 June 2008 / Accepted: 12 March 2009
© Springer Science+Business Media B.V. 2009

Abstract Analysis of capillary-pressure distribution in single channels with sinusoidal profile shows that surface tension-driven flow in such channels is controlled by the pressure extrema at their crests and troughs. Formulating the geometric condition for the pressure in the troughs to exceed that in the crests leads to a simple criterion for the spontaneous break-up of the non-wetting fluid in the necks of the constrictions. The criterion reduces to the condition for the Plateau-Rayleigh instability as a limiting case. Similar pressure analysis is applicable to the case of a non-wetting fluid invading an open pore body. Computational-fluid-dynamics experiments have verified the validity of the break-up predicted from the capillary-pressure argument. Although the geometric criterion for the break-up is valid for small capillary numbers, it provides a common framework in which the results of various published studies of a non-wetting phase choke-off in capillary constrictions for a wide range of capillary numbers can be explained and understood.

Keywords Fluid break-up · Instability · Capillary flow · Porous channels

Electronic supplementary material The online version of this article (doi:10.1007/s11242-009-9381-6) contains supplementary material, which is available to authorized users.

I. A. Beresnev 

Department of Geological and Atmospheric Sciences, Iowa State University, 253 Science I, Ames, IA 50011-3212, USA
e-mail: beresnev@iastate.edu

W. Li

Pfizer Global Research and Development, 600 Eastern Point Road, MS 8260-2121, Groton, CT 06340, USA
e-mail: wenqing.li@pfizer.com

R. D. Vigil

Department of Chemical and Biological Engineering, Iowa State University, 2114 Sweeney Hall, Ames, IA 50011-2230, USA
e-mail: vigil@iastate.edu

1 Introduction

Spontaneous surface tension-driven break-up of immiscible non-wetting fluids into isolated drops in sinusoidally constricted channels has been subject of several studies, with the focus on revealing the conditions under which it occurs (Obricht and Leal 1983; Tsai and Miksis 1994; Hemmat and Borhan 1996; Gauglitz and Radke 1990). The interest has been caused by the phenomenon's technological applications arising in petroleum recovery and chemical engineering (foam and mono-disperse emulsion formation). In formulating such conditions, the fact has often been overlooked that the geometry of the constriction plays a fundamental role in determining if the fluid breaks up into beads or remains continuous, while the characteristics of the fluid itself and the flow can only promote or impede the break-up already prescribed by the geometry.

The interpretation of the conditions for the break-up in terms of just the flow parameters, out of the context of the geometry, can be misleading, as it seeks the explanation of the phenomenon in the factors other than its true causes, making it appear all but enigmatic why the break-up occurs in some cases but not in the others. Hemmat and Borhan (p. 383) directly indicate, for example, as the conclusion to their experiments that "the role of the capillary geometry in determining the critical conditions for the onset of drop breakup warrants further investigation". On the other hand, realizing that the geometry is the most important factor controlling the fluid disintegration could provide a unifying framework in which results of miscellaneous observations could be related and understood.

Another group of studies, acknowledging the critical role of geometry, attempts to reduce the criterion for the snap-off to just the ratio of the minimum and maximum channel radii (Rossen 2003; Kovscek et al. 2007). This condition would also be incomplete, because it neglects the presence of a channel's wavelength, which enters as another important controlling parameter. The full description would invoke all three geometric parameters and has never been explicitly formulated.

This study is devoted to realizing this goal. It derives the geometric condition for the spontaneous snap-off of a non-wetting fluid in a sinusoidally constricted capillary and demonstrates that it succeeds in explaining the results of various published studies. The theoretically deduced condition is verified in a computational-fluid-dynamics experiment.

2 Geometry of the Problem

We are concerned with an axisymmetric capillary channel having a sinusoidal profile as depicted in Fig.1. In the cylindrical coordinates, the channel profile is defined by the following equation:

$$r(z) = r_{\max} \left[1 + \frac{1}{2} \left(\frac{r_{\min}}{r_{\max}} - 1 \right) \left(1 + \cos \pi \frac{z}{L} \right) \right], \quad (1)$$

where r_{\min} and r_{\max} are the minimum and the maximum radii, and $2L$ is the spatial period. The channel is filled with a non-wetting core fluid, and an assumption is made that a thin film of a wetting fluid separates the non-wetting phase from the channel wall. In typical oil recovery applications, the non-wetting core phase would be oil and the wetting phase would be water. Our analysis will assume small capillary numbers (Ca), at which the deformation of the oil phase due to viscous forces can be neglected.

We start with deriving the condition for the break-up for the case of the oil totally filling the channel, and then will discuss how the analysis changes for the case of oil invading a

Fig. 1 Geometry of the problem

water-occupied pore body (drainage). A common terminology will be used, in which a "pore body" is the open space with the maximum radius contained between two constrictions, and the constriction itself is a "pore throat".

3 Simple Static Criterion for the Break-up: The Non-Wetting Fluid Filling the Channel

The spontaneous break-up of fluid streams and jets is driven by capillary forces, which arise due to variation in the capillary-pressure along the boundaries. In the wetting film, the pressure is approximately constant across its thickness (Lesslö 1997 art. 330). Furthermore, if the film is sufficiently thin (at the initial stages of the development of the collars of water that will eventually complete the snap-off), it is also reasonable to assume that there are no pressure gradients in the film along the solid wall either. There are three observations that support this conclusion. First, if such internal gradients existed, for example, the water completely filling a corrugated channel would spontaneously circulate, which is certainly not the case. This is physically well justified, of course, because the surface of a wetting fluid in contact with a solid wall does not possess any extra energy (the definition of "wetting"), and therefore no significant capillary forces exist at this surface. Second, the absence of internal gradients is evidenced by the stability of water coatings spread over wettable substrates (e.g., glass). This stability can be understood in terms of the constant pressure within them; any internal gradients would inevitably force recirculation and break-up, but such wetting films are observed not to disintegrate spontaneously. Third, in an unconfined immiscible environment, oil droplets inevitably take the form of spherical globules. The fact that the end result is independent of the surrounding phase, be it air under constant atmospheric pressure or fluid, supports the view that, to describe the final state, the pressure in the surrounding phase can be considered constant and the process driven solely by the internal pressures in the oil. We thus arrive at the conclusion that the pressure in the surrounding phase is approximately uniform for the purposes of our analysis. Note that a similar premise was used by Saffman (1961, p. 167) and Middleman (1995 p. 60).

With this observation in mind, the evolution of the fluid-fluid interface can be considered to be controlled by the pressure gradients in the core, while the film responds passively. Note that, in explaining the physical reasons for the break-up of a fluid, Rof (1970) took a similar approach, in which the oil snap-off was assumed to be caused solely by the gradients in

the core pressure; the author nevertheless provided no physical reasons why the pressure in the film could be taken constant. Roof (1970, p. 88) found reasonable agreement between the experimentally observed distance traveled by an oil interface through a given geometry before it snapped off and the theoretically predicted value based on the differences in core pressure, which validates his point.

The pressure in the oil, relative to water, is described by the Laplace equation

$$P_{ca} = \sigma (1/R_1 + 1/R_2), \tag{2}$$

where P_{ca} is the capillary-pressure, σ is the oil/water interfacial tension, and $1/R_1$ and $1/R_2$ are the principal curvatures of the channel surface (those of two mutually orthogonal principal normal sections R_1 and R_2 are the principal radii of curvature). The curvature is considered positive under a convex surface (such as one under the crests of the profile in Fig. 1, at $z/L = 1$), as it then correctly leads to a pressure increase, and negative under a concave surface (under the troughs; e.g., at $z = 0$). Note that a sum of any two normal curvatures (corresponding to any pair of mutually orthogonal normal sections) can be taken in Eq. (Graustein 2006, p. 113).

Let us consider two cross-sections perpendicular to the channel axis: one at its maximum radius (the crest) and another at its minimum radius (the trough) (the cross-sections with r_{max} and r_{min} in Fig. 1). As it is clear from the geometry, at the crest, both normal curvatures are positive. One (in the plane perpendicular to that of Fig. 1) equals $1/r_{max}$ and the other (in the plane of Fig. 1) is the curvature of the sinusoidal profile, (which, as seen from its general form (A-6), equals $\frac{\pi^2 r_{max}}{2L^2} (1 \mp \frac{r_{min}}{r_{max}})$), with the correct sign chosen. The capillary-pressure at the crest therefore is

$$P_{ca}^{crest} = \sigma \left[\frac{1}{r_{max}} + \frac{\pi^2 r_{max}}{2L^2} \left(1 \mp \frac{r_{min}}{r_{max}} \right) \right]. \tag{3}$$

If we now turn to the trough, one normal curvature is still positive ($1/r_{min}$), but the other is negative but still has the same absolute value as that at the crest (the saddle shape). The capillary-pressure at the trough becomes

$$P_{ca}^{trough} = \sigma \left[\frac{1}{r_{min}} \mp \frac{\pi^2 r_{max}}{2L^2} \left(1 \mp \frac{r_{min}}{r_{max}} \right) \right]. \tag{4}$$

If the pressure at the neck of the constriction exceeds that at the crest, the resulting pressure difference, equal to

$$P_{ca}^{trough} \mp P_{ca}^{crest} = \sigma \left[\frac{1}{r_{min}} \mp \frac{1}{r_{max}} \mp \frac{\pi^2 r_{max}}{L^2} \left(1 \mp \frac{r_{min}}{r_{max}} \right) \right], \tag{5}$$

will drive the non-wetting fluid out of the neck toward the crest of the profile, with an accompanying invasion of the wetting fluid into the neck and the resulting pinch-off (Roof 1970).

The condition for this gradient to form is $P_{ca}^{trough} > P_{ca}^{crest}$, or, from Eq 5,

$$\lambda > 2\pi \frac{1}{r_{min} r_{max}}. \tag{6}$$

We will call condition (6) the *static* criterion for the oil break-up in the neck. It is evidently controlled by the geometry only and has not appeared in the earlier literature (Roose 2003; Kovscek et al. 2007). We use the word *static* throughout the manuscript to emphasize the point that the analysis strictly applies to a stationary problem. As long as the capillary number is small, the interfacial forces dominate the flow and this assumption remains justified. The stationary problem also assumes that sufficient inflow of water is available into the neck

to complete the snap-off. As we will see in the sections verifying the applicability of this analysis using numerical simulations and available experimental data, it agrees with the data even at finite capillary numbers.

It also should be noted that we limit ourselves to single constricted channels only and leave out possible modifications due to pore connectivity (Rossetti 2003)

Strictly speaking, condition (6) applies to the onset of instability while the Plateau is still thin enough. When the oil starts to flow and the water collar in the neck starts to grow, the assumption of a uniform pressure in the wetting phase will eventually break down. The collar growth will cause p_{min} to tend to zero, while p_{max} will remain by order of magnitude the same. The condition (6) for the oil pressure in the neck to exceed that in the crest will therefore still be valid, ensuring continuous outflow of oil. It is thus reasonable to expect that this condition, although formally valid for the onset of break-up only, will still be sufficient to cause the complete snap-off. Indeed, all literature results surveyed below, as well as our own CFD simulations also shown in a later section, indicate that meeting the onset criterion leads to the eventual pinch-off.

In the limiting case of $r_{min} = r_{max} = R$, criterion (6) simplifies to $\lambda > 2\pi R$, which is the well known shortest wavelength to cause the instability of a liquid cylinder (the Plateau-Rayleigh instability) (de Gennes et al. 2004 Eq. 5.22). If R is the radius of the core, the Plateau-Rayleigh formula also describes unstable wavelengths for the core-annular flow in straight cylinders, which can be deduced from the respective expressions (Chapman and Crawford (1983 Eqs. 2.23-2.24). Our condition (6) thus correctly converges to the known limiting cases. Re-writing (6) in the form $\frac{\lambda}{2\pi r_{min}} \frac{\lambda}{2\pi r_{max}} > 1$ imparts it a simple geometric meaning: its left-hand side represents a product of the ratios of the wavelength to the minimum and the maximum circumferences of the tube.

One also may note that, if we have the opposite condition satisfied, $p_{ca}^{trough} < p_{ca}^{crest}$, the core fluid will flow out from the crests into the neck seeking a stable configuration, which will eventually be reached due to geometric confinement provided by the wall or if the radii r_{min} and r_{max} can be equalized.

Condition (6), establishing the pressure gradient causing the outflow of oil from the neck of the constriction, was obtained without regard to other possible intermediate pressure highs and lows between the troughs and the crests of the profile. If they exist, the oil-flow pattern may be more complex and not necessarily lead to the pinch-off at the neck. To prove the general validity of criterion (6), one would have to show that the pressures at the neck and the crest indeed control the pressure gradient in the oil phase. To that end, a general expression for the principal curvatures at an arbitrary point on the channel surface should be obtained. This expression is derived in Appendix A, and Appendix B proves the dominance of the capillary-pressure in the troughs and crests over any other intermediate extrema for the parameter combinations that allow analytical treatment. These parameter combinations cover a great portion of the parameter space but of course not all of it. A general proof does not seem feasible due to the complexity of algebraic equation (3). The existence of intermediate extrema and the value of capillary-pressure at them relative to that in the troughs and crests can of course always be established graphically for any particular parameter combination, by directly plotting expression (B-1). An example of such an analysis is provided in the next section.

4 Illustration of the Criterion Validity

We would like to illustrate the capillary-pressure distribution along the channel for the conditions at which criterion (6) is and is not satisfied. In the numerical example, we choose

Fig. 2 Capillary-pressure distribution along the channel for $r_{\max} = 0.1$ mm and $r_{\min} = 0.01$ mm. a $\lambda/(2\pi \sqrt{r_{\min}r_{\max}}) = 3$, b $\lambda/(2\pi \sqrt{r_{\min}r_{\max}}) = 0.5$

and r_{\min} of 0.1 and 0.01 mm to represent the typical pore sizes encountered in oil-bearing reservoirs. Representing condition (6) as $\lambda/(2\pi \sqrt{r_{\min}r_{\max}}) > 1$, we calculate the capillary-pressure using Eq. B-1 for the values of 3 and 0.5 of the ratio on the left-hand side. The former case should therefore lead to the pinch-off at the neck and the latter to the fluid outflow from the crest toward a stable configuration. The channel wavelength in the two cases is 0.60 and 0.099 mm, respectively. The calculated pressure profiles are depicted in Fig. 2 if $\sigma = 0.040$ N/m.

For the geometry used in the example, $r_{\min} \ll r_{\max}$ and $r_{\max} \ll L$. From the approximate analysis provided in Appendix B, the intermediate extrema therefore exist but they do not dominate the flow, which is consistent with the curves in Fig. 2. The coordinates of these extrema that fall within the limits of applicability of Eq. B-11 should be the solutions of this equation. For the geometry in Fig. 2a, Eq. B-11 yields $\cos\tau(z/L) = \sqrt{1.2}$ and has no roots. The local minima are nevertheless seen in Fig. 2a between z/L of 0.5 and 1, and 1 and 1.5. This shows that they fall out of the range of the validity of Eq. B-11, due to the neglect of higher powers of cosine used in deriving Eq. B-11). On the other hand, for the geometry in Fig. 2b, Eq. B-11 gives $\cos\tau(z/L) = \sqrt{0.033}$, which has two roots, $z/L = 0.51$ and 1.49, in the range of z/L shown in Fig. 2b. These "shallow" local minima are indeed present in Fig. 2b. Two "gentle" local maxima can also be observed, between 0 and 0.5, and 1.5 and 2. The approximate analysis, for the same reason, was unable to capture these maxima as well.

The curves in Fig. 2 demonstrate the validity of the static criterion. According to condition (6), capillary-pressure has distinct peaks at the necks of the constrictions ($z = 0, 2$) in

Fig. 2a, which will cause the fluid pinch-off at the necks. On the other hand, the opposite condition is satisfied in Fig. 2b, causing the peaks in the capillary-pressure at the crests (1) and sinks at the throats. The outflow of fluid from the crests into the throats can thus be expected. The effect of intermediate extrema in either case is insignificant.

5 Modification of the Analysis for the Non-Wetting Fluid Invading a Pore Body (The Drainage Case)

The geometric conditions for the spontaneous break-up have so far been established and verified for the non-wetting fluid filling the channel. From the practical standpoint, the case of the oil invading a water-occupied pore body (the drainage scenario) would also be important. One should see how the analysis of the conditions for the break-up should be modified for such a new situation. For simplicity, complete non-wetting by oil (zero contact angle) will be considered. We will also assume the static condition, that is, neglect the disturbance of the pressure field in water by the invading meniscus, this is possible because we neglect viscous effects under the assumption of small capillary number.

For an invading non-wetting (spherical) meniscus, two cases should be distinguished as illustrated in Fig. 3. In Fig. 3a, the curvature of the wall is sufficiently small that the moving meniscus (two positions are shown) never intersects the wall. In this case, the invading oil is always bounded by two interfaces: the solid wall and the spherical oil-water front tangent to the wall at the three-phase contact line (at the axial coordinate

This case is different from that in Fig. 3b, in which the curvature of the wall is large enough to cause the invading meniscus to intersect the wall as it advances into the pore body. The first configuration in Fig. 3b shows the still completely spherical invading meniscus when it first touches the opposite (descending) wall. Following that moment, the previously continuous meniscus splits up as shown by the second configuration: part of it continues to move

Fig. 3 Possible meniscus geometries for a non-wetting fluid invading a pore body (the motion is from left to right).
 a Spherical meniscus not intersecting the wall
 b spherical meniscus intersecting the wall

forward as the leading spherical front CC, but a remnant of it advances toward the crests of the pore as indicated by surfaces AB. These split menisci are separated by the solid wall along surfaces BC. Note that the interfaces AB represent caps of tori formed as surfaces of revolution of the circular arc AB about the axis. The oil is thus bounded by sections of the solid wall, toroidal menisci AB, and the spherical front CC.

The cases in Figs 3a and b are distinguished by the no-intersection condition,

$$\frac{2L^2}{\pi^2 r_{\max}(r_{\max} \dot{\sim} r_{\min})} > 1 \tag{7}$$

(Beresnev 2006 Eq.5), namely if inequality (7) holds, the spherical meniscus does not intersect the wall. We further analyze the capillary-pressure in these two cases separately.

5.1 The Invading Meniscus not Intersecting the Wall

The radius R_m of the sliding spherical meniscus in Fig 3a is related to α_c as

$$R_m(z_c) = r(z_c)\sqrt{1 + r'^2(z_c)}, \tag{8}$$

and the capillary-pressure on the oil side is

$$P_{ca}^m(z_c) = 2\sigma/R_m(z_c). \tag{9}$$

Let us re-consider the case of Fig 3a in which this invading meniscus is now present. The no-intersection condition (7) reads $2 \times (0.3 \text{ mm})^2 / [\pi^2 \times (0.1 \text{ mm}) \times (0.1 \text{ mm} \dot{\sim} 0.01 \text{ mm})] = 2.0$, and is satisfied. In addition to the pressure distribution along the channel from Fig. 2a, we now need to take into account the pressure at the invading front. Figure 4a shows both: (i) it reproduces the curve from Fig 2a (thin line) and (ii) compares it with Eq. (9) (bold line) where the axial coordinate is that of the sliding contact line. These two curves should be interpreted as follows. Recalling the invasion geometry in Fig. 3a, every point on the bold line represents a constant oil pressure at the invading spherical front for a given front leaves a pressure distribution behind (to the left, shown by the thin line). Figure 4a therefore indicates that, up to a certain value of L (about 0.2), the pressure at the front is always greater than the pressure at any point behind it. However, when the front passes that point, its pressure drops below the capillary-pressure at the neck ($= 0$). This creates the condition for the break-up at the neck, which holds until the pressure at the moving front is again above the value at the neck, which occurs at L of about 1.8. The conditions for the break-up at the neck thus exist as long as the moving front is between 0.2 and 1.8. This modifies the analysis, previously presented in Fig. 2a for the case of an invading, non-intersecting meniscus.

5.2 The Invading Meniscus Intersecting the Wall

In the case of Fig 3b, the right-hand side of the no-intersection condition is 0.055, and the condition is not satisfied. This case should thus be re-considered in the framework of the geometry illustrated in Fig 3b.

Figure 4b reproduces the curve from Fig 2b (thin line), and it also shows the capillary-pressure at the invading spherical front as two segments, before and after it touches the wall (two segments of bold line). The bold lines are still calculated using Eq. (9). As Fig. 3b illustrates, there is no contact line of the spherical front between points D and E, which is reflected in the separation of the two bold segments. Instead, when the front meniscus is at contact

Fig. 4 Capillary-pressure analysis for the case of an invading meniscus. *Thin lines* reproduce pressure distributions from Fig2; *bold lines* are pressures at the invading spherical meniscus. a, spherical front not intersecting the wall, b spherical front intersecting the wall

Fig. 5 Geometry of the circular arc forming the upper and lower menisci in Fig3b

point E and beyond, separate, toroidal menisci exist as the surfaces AB. The full analysis should thus include the capillary-pressure at these interfaces.

The torus-forming circular arc AB is reproduced in Fig5 where R_t is its radius and z_L is the coordinate of its left contact line. From the geometry, $r = L \sin \theta$, or, considering that $\tan \theta = r(z)$ (as in Fig.A-1),

$$R_t(z_L) = (L \sin \theta) \frac{\sqrt{1 + r^2(z_L)}}{r(z_L)}. \tag{10}$$

As also seen in Fig. 5, the r -coordinate of the center of this circle is $r_0(z_L) = r(z_L) \check{S} R_t \cos \theta$, which, using (10), yields

$$r_0(z_L) = r(z_L) \check{S} \frac{L \check{S} z_L}{r(z_L)}. \tag{11}$$

Note that expression (10) can be used to find the coordinate of point D in Fig. 3b (z_D) at which the invading meniscus first touches the opposing wall. Indeed, in this situation, r_0 becomes R_m . Consequently, by replacing r_0 in the right-hand side of Eq. (10) by R_m from Eq. 8, one obtains a nonlinear algebraic equation that can be solved numerically. For example, for the geometry of the example in Fig. 4b, this solution is $z_D/L = 0.23$. This is the coordinate at which the left segment of the bold line ends in Fig. 4b.

The parametric equation of the torus formed by the revolution of a circle with radius a about an axis that is a distance b from the center of the circle ($a > b$) is

$$x(u, v) = (a + b \cos u) \cos v, \tag{12a}$$

$$y(u, v) = (a + b \cos u) \sin v, \tag{12b}$$

$$z(u, v) = b \sin u \tag{12c}$$

(cf. Eq. A-1). To find the principal curvatures, we can follow the approach outlined in Appendix A. Using the formulae from Appendix A, the coefficients F , G , L , M , and N of the first and second fundamental quadratic forms of the surface (12) are b^2 , $F = 0$, $G = (a + b \cos u)^2$, $L = b$, $M = 0$, and $N = (a + b \cos u) \cos u$. From these values, the sum of the principal curvatures for the torus is found as

$$\frac{1}{R_1} + \frac{1}{R_2} = \frac{a + 2b \cos u}{b(a + b \cos u)}, \tag{13}$$

which can be used in Eq. 2 to calculate the capillary-pressure. It is useful to determine the behavior of capillary-pressure along the surface of the torus; for example, to determine the minima and maxima of P_{ca} . To this end, we take the derivative of Eq. 13 with respect to u and equate it to zero, which leads to the equation $\sin u = 0$. The extrema of the capillary-pressure thus occur at $u = 0, \pi$, which correspond to the outer and the inner rings of the torus (12), respectively. To further find out which of these extrema is the maximum and which is the minimum, we take the difference of the values of Eq. 13 calculated at $u = 0$ and $u = \pi$: $(a + 2b) / [b(a + b)] \check{S} (a \check{S} 2b) / [b(a \check{S} b)] = 2a / [(a + b)(a \check{S} b)]$. Considering that $a > b$, the right-hand side is always positive, showing that the sum of the principal curvatures (13) has its maximum at $u = 0$ and the minimum at $u = \pi$. This means the capillary-pressure under the toroidal surface monotonously decreases from its maximum at the outer ring corresponding to the crest of the profile in Fig. 3b. This result was of course intuitively clear, considering that both principal curvatures at the outer ring of the torus are positive, and one is positive and the same at the inner ring while the other is negative (the saddle shape).

We now can determine the position of the toroidal meniscus AB in Fig. 3b as the spherical front CC progresses toward the throat ahead. We observe that the new position of the meniscus AB for a given position of the spherical front is reached when the maximum pressure at AB equals the pressure at the spherical front. The maximum pressure under the toroidal surface is found from Eq. 13 at $u = 0$. Considering that, in the notation of Fig. 4b, $b = R_t$ and $a = r_0$, the maximum pressure is

$$P_t(z_L) = \sigma \frac{r_0(z_L) + 2R_t(z_L)}{R_t(z_L) [r_0(z_L) + R_t(z_L)]}, \tag{14}$$

where R_t and r_0 are defined by Eq. 10 and 11, respectively. Note that, although h is not necessarily greater than r_0 in our case, the capillary-pressure still has its maximum at the crest of the profile. Since we are dealing with only part of the toroidal surface formed by the circular arc in Fig. 5, this simply means there is maximum but no minimum of the pressure over this surface. Equating pressure (to the pressure at the spherical front CC at given position of its contact line c_c (Eq. 9), we obtain a nonlinear algebraic equation for the position z_L of the left contact line of the toroid AB (the coordinate of point A in Fig. 3b) corresponding to z_c ,

$$\frac{r_0(z_L) + 2R_t(z_L)}{R_t(z_L) [r_0(z_L) + R_t(z_L)]} = \frac{2}{R_m(z_c)}. \quad (15)$$

This equation can be solved numerically. For example, when the spherical front advances half of the distance between its initial position (contact point at E) to the neck of the constriction ahead (the right end of Fig. 3b) [this location is indicated as the dot labeled $\dot{O}3\dot{O}$ on the ascending bold line in Fig. 4b: $z_c/L = 2 \dot{S} (z_D/L)/2 = 2 \dot{S} [0.23/2]$], the solution of Eq. 15 is $z_L/L = 0.84$. This is the respective position of the left contact line of the upper toroidal meniscus, as shown as dot $\dot{O}1\dot{O}$ on the thin line in Fig. 4b. Dot $\dot{O}2\dot{O}$ is therefore the location of the right contact line. Since dots $\dot{O}1\dot{O}$ and $\dot{O}2\dot{O}$ bracket the location of the upper meniscus, the capillary-pressure outside the bracketed interval follows the thin line in Fig. 4b. Note that, when the spherical front advances to its extreme right position, with its contact line CC touching the wall exactly in the neck of the constriction ahead, there is no solution to Eq. 15. The capillary-pressure at the front in this case is 8,000 Pa (the value of the bold ascending line in Fig. 4b at $z_c/L = 2$). The absence of the solution means that this pressure is higher than the maximum pressure at any position of the upper toroidal meniscus; in other words, by this time the toroidal meniscus has disappeared and the non-wetting fluid has entirely filled the pore body. Indeed, the maximum of Eq. 14 at any z_L for which the upper meniscus exists (z_L/L between 0.23 and 1) is 7,600 Pa. The capillary-pressure behind the front at this time then just follows the uninterrupted thin line in Fig. 4b.

With the exact positions of all menisci thus known, Fig. 4b then should be interpreted in the same way as Fig. 4a. One can see that the pressure at the moving spherical front at any time is greater than or equal to the pressure at any point behind it. This shows that, unlike the situation of the continuous fluid distribution (Fig. 2b), no outflow of the fluid from the crests of the profile leading to a respective reconfiguration of the interface there can now be expected. This modifies the analysis, presented in Fig. 2b, for the case of an invading meniscus intersecting the wall.

6 Validation of the Criterion in a Numerical Experiment

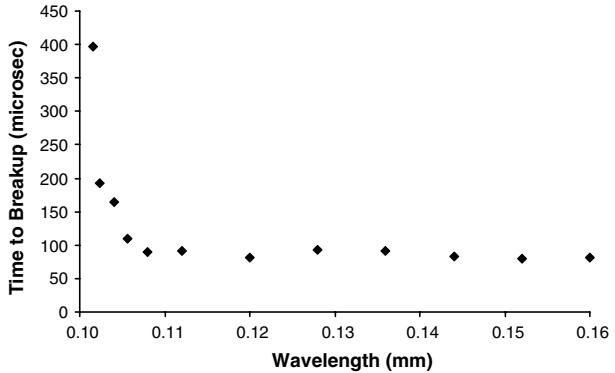
The validity of criterion (6) for the spontaneous break-up of a non-wetting fluid in the neck of the constriction was verified in a numerical experiment using the finite-volume computational-fluid-dynamics code FLUENT. A large ganglion of the non-wetting phase was inserted symmetrically between two adjacent pore bodies, completely filling the throat as indicated in Fig. 6 (top), in the absence of external forces, and the temporal evolution of the shape of the drop, driven by capillary forces alone, was computed. The ganglion was surrounded by a continuous wetting phase.

The simulations were run in FLUENT's Volume of Fraction (VOF) axisymmetric model for the immiscible multi-phase flow. The mesh-generation software GAMBIT was used to construct a 65 (radial) \times 481 (axial) mesh on which the axial and radial momentum,

Fig. 6 Computational-fluid-dynamics simulation of the evolution of the shape of a ganglion of non-wetting fluid initially filling the pore constriction. Time in microseconds is indicated beside each frame

continuity, and volume-fraction equations were solved. The following solution schemes for the VOF model were applied: the PREssure STaggering Option (PRESTO) for pressure interpolation, the second-order discretization for the volume-fraction equation, the Pressure Implicit with Splitting of Operators (PISO) scheme for pressure-velocity coupling, and the second-order upwind discretization for the momentum equations. The segregated

Fig. 7 Dependence of the time to snap-off on the tube wavelength $\lambda = 2L$



solver provided by FLUENT solves the governing equations sequentially. Grid spacing was non-uniformly distributed in the radial direction to provide better resolution near the wall, and was uniform in the axial direction. The flow was assumed incompressible, and the no-slip boundary condition was applied at the wall. The density and viscosity of water were 998 kg/m^3 and $10^{-3} \text{ Pa}\cdot\text{s}$, and the density and viscosity ratios of unity between oil and water were assumed. The interfacial tension was 0.0345 N/m . Grid refinement studies were performed to ensure that the computed profiles and times to break-up were grid-independent. The total time to compute Fig. 6 and similar results was about 20h on a 2.4-GHz workstation.

The sinusoidal tube consisted of six complete periods (not shown in Fig. 6) with r_{max} and r_{min} of 0.03 and 0.01 mm, respectively. A water film of uniform thickness of 0.0025 mm (one-fourth of r_{min}) separated the oil from the pore walls at the start of the simulations.

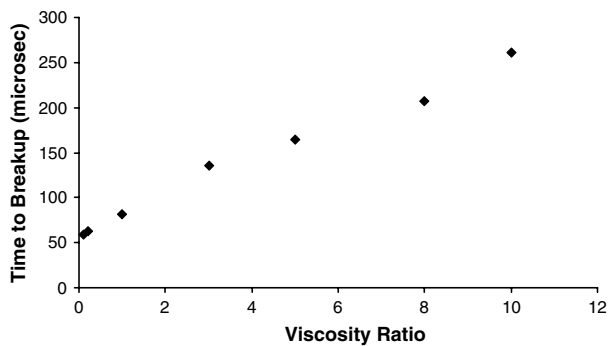
From Eq. 6 for the given values of r_{max} and r_{min} , taking the thickness of the wetting film into account, the spontaneous break-up was expected at wavelengths $(0.03 \pm 0.0025)(0.01 \pm 0.0025)^{1/2} = 0.0902 \text{ mm}$. A series of simulations were run for the values of λ bracketing this presumed snap-off threshold to observe the range of transition from no break-up to break-up, as summarized in Table 1. The numerically calculated snap-off took place between λ of 0.1008 and 0.1016 mm. Taking their average of 0.1012 mm, this wavelength is 0.0110 mm, or about 12%, larger than the theoretical prediction, which can be viewed as a reasonable agreement. This fully dynamic simulation corroborates the geometric argument that the conditions for the break-up, established by criterion (6), are (mainly) valid even though the criterion strictly applies to the onset of instability when the collars only start to form.

Figure 6 illustrates the entire process of choke-off, computed for the wavelength of 0.12 mm. The calculated time to break-up (complete separation of the two satellite drops) is $82 \mu\text{s}$. A complete computed movie of the process is available from the mpeg file attached (see electronic supplement to the paper).

We also investigated the dependence of the time to break-up on the tube wavelength (within the range where it occurred) and the viscosity ratio between the two phases. As Fig. 7 illustrates, this time decreases steeply with increasing wavelength and then levels off. This behavior can be qualitatively understood in terms of the pressure difference Δp that drives the snap-off. For fixed r_{max} and r_{min} , the pressure difference increases quickly with increasing wavelength, with the quadratic dependence $\Delta p \propto \lambda^2$, leading to quicker break-up. When the third term in the brackets of Eq. 6, however, becomes sufficiently small compared to the sum of the first two terms, the pressure difference levels off.

Table 1 Numerical testing of the static break-up criterion

Wavelength (mm)	Break-up occurred
0.1600	Yes
0.1520	Yes
0.1440	Yes
0.1360	Yes
0.1280	Yes
0.1200	Yes
0.1120	Yes
0.1080	Yes
0.1056	Yes
0.1040	Yes
0.1024	Yes
0.1016	Yes
0.1008	No
0.1000	No
0.0984	No
0.0960	No
0.0920	No
0.0902	No
0.0890	No

Fig. 8 Dependence of the time to snap-off on the viscosity ratio between the drop and the suspending phase ($\lambda = 0.12$ mm)

The dependence on the viscosity ratio between the drop and the suspending phase is illustrated in Fig.8, for the wavelength of 0.12 mm. The viscosity of the wetting phase is always kept at 10^{-3} Pa.s. The observed near-linear increase in the time with increasing viscosity of the drop phase could be expected, as, for the same driving forcing, the deformation is slower for the more viscous drop. One nevertheless should keep in mind that, although Figs. 8 show the specific dependencies, the values of the time to snap-off can be expected to vary by orders of magnitude depending on the initial thickness of the water film and the values of r_{\max} and r_{\min} (e.g., Gauglitz and Radke 1990, their Fig. 12). Computational restrictions have limited so far our further exploration of the parameter space; it should be kept in mind that one point in either Figs. 7 and 8 or Table 1 requires at least several hours of CPU time.

Table 2 Summary of published results on break-up observation in sinusoidal capillary tubes

	Type of study	$\frac{\lambda}{2\pi r_{\min}r_{\max}}$	Static criterion satisfied?	Snap-off observed?
Tsai and Miksis(1994)	Numerical model	0.38, 0.45, 0.50, 1.0	No	No at small Ca
Hemmat and Borha(1996)	Experiment	1.3	Yes	Yes
Olbricht and Lea(1983)	Experiment	0.71	No	No at small Ca
Martinez and Udel(1989)	Numerical model	0.71, 0.92	No	No
Gauglitz and Radke(1990)	Numerical model and experiment	4.5, 5.7, 7.1	Yes	Yes

7 Analysis of Published Results

As indicated in Introduction, several studies investigated the immiscible flow and choke-off of non-wetting fluids in sinusoidally constricted single tubes, albeit without addressing a unifying geometrical condition for the spontaneous choke-off to occur. Our intention is to verify if these observations can be understood through the break-up criterion (6)

Table 2 summarizes the results of published break-up observations; it also indicates in column 2 whether this was a theoretical or experimental work. As shown in Table 2, all investigations observed an actual break-up, or the latter happened under certain conditions only. To put all the results in a common perspective, we calculated the ratio $\frac{\lambda}{2\pi r_{\min}r_{\max}}$ from criterion (6) for each of the studies (some presented results for several ratios), which are shown in column 3. Recall that the snap-off should be observed if $\frac{\lambda}{2\pi r_{\min}r_{\max}} > 1$. Column 4 then simply states if this inequality was satisfied, and the last column indicates if the snap-off was or was not observed.

One can see that the results of Table 2 are consistent with the static break-up criterion, in that the studies in which the inequality was not satisfied did not document the snap-off. The only deviations from this rule occur in the results reported by Olbricht and Lea (1983) and Tsai and Miksis (1994). Specifically, in these two studies, the criterion was not satisfied, and the snap-off was not observed at small capillary numbers but it did occur at large capillary numbers. Olbricht and Lea (1983) reported no break-up for $Ca = 0.08$, and Tsai and Miksis (1994) for $Ca < 0.03$.

In explaining these deviations, one should recall that significant elongation of the ganglia of non-wetting phase moving through capillary channels is observed at large capillary numbers, increasing the thickness of the wetting film in the constrictions and thereby reducing the effective value of r_{\min} , facilitating the snap-off. A snap-off that is observed at greater capillary numbers, even if the static criterion is not satisfied, can thus disappear at smaller ones. An example of such a transition is given by Tsai and Miksis (1994) in their Figs. 8 and 9). In this example, the same ganglion experienced a snap-off at $Ca = 0.1$ but did not break at $Ca = 0.05$. Note that the static criterion was not satisfied (Table 2). Another factor for realistic systems is the length of the oil phase. The snap-off, being a dynamic process, requires a finite time to develop, through the growth of the wetting collar in the constriction that eventually chokes-off the oil. Even if the snap-off is allowed by the geometry, it may not actually occur due to a short residence time of oil in the constriction if the length of the oil phase is sufficiently small. For instance, in the example of Tsai and Miksis, the choke-off that was geometrically allowed at $Ca = 0.1$ because of the sufficient thickness of the water film in the throat (small r_{\min}), was inhibited again at $Ca = 0.2$, because the increased flow

rate of the oil ganglion made its residence time in the throat too short. On the other hand, the residence time could be increased by simply increasing the length. An example of this kind is also discussed by Tsai and Miksis (1994, their Figs. 9 and 11). The ganglion did not break at $Ca = 0.05$ for the reasons already considered, while a longer ganglion did for the same capillary number. The snap-off in large-capillary-number systems thus becomes the result of a trade-off between the thickness of the water Plm and the oil-phase residence time: with growing Ca , the Plm in the throat is thicker but the residence time is shorter. Note that capillary numbers in oil-recovery applications are much smaller, on the order of 10^{-5} to 10^{-8} (e.g., Melrose and Brandner 1974, 58), which makes the static criterion universally applicable to them.

8 Conclusion

Capillary-pressure analysis at the crests and troughs of single channels with sinusoidal geometry filled with a non-wetting fluid shows that the pressure at these locations typically controls the spontaneous, surface tension-driven flow. Formulation of the geometric condition at which the capillary-pressure peaks at the troughs of the profile (the necks of the constrictions) then leads to a purely geometric criterion for the spontaneous break-up at the necks in form of Eq. 6. In the limiting case of cylindrical streams with a free boundary and cylindrical core-annular flows, this criterion reduces to the condition for the occurrence of the Plateau-Rayleigh instability. If the opposite inequality is satisfied, it becomes the condition for the dissipation of the disturbance imposed by the solid wall. The pressure analysis for a non-wetting fluid invading a pore body should only be modified to include the presence of an additional interface (the invading meniscus), with the distinction made between the geometries in which this meniscus intersects and does not intersect the wall of the pore.

Criterion (6) explains how the snap-off mechanism described by Roy (1970) can lead to the break-up of continuous non-wetting core streams in some periodic channels but not in the others, a contentious point having received no earlier explanation in the literature. It brings to the forefront the fact that the channel's wavelength, in its relation to the minimum and maximum radii, and not the radii alone, is the key controlling factor. We have also placed the derivation of the criterion on a more rigorous physical basis justifying why the pressure in the wetting Plm could be for this purpose considered constant, which allows to use the pressure gradients in the core alone as those driving the snap-off.

This geometry-controlled condition for the fluid break-up, which has never appeared in the literature before, is valid at small capillary numbers and is validated in a computational experiment. It also provides a unifying approach to explaining the results of various published experimental and theoretical studies of immiscible flow in single sinusoidal channels, both at small and large capillary numbers.

Acknowledgments This study was supported by the National Science Foundation and the Petroleum Research Fund. Proper acknowledgment is made to the donors of the American Chemical Society Petroleum Research Fund.

Appendix A: Principal Curvatures at an Arbitrary Point on the Channel Surface

The normal curvatures of a surface of revolution such as one depicted in Fig. 1 are not as obvious as they may seem. One (in the plane of Fig. 1) clearly the curvature of the sinusoidal wall profile (1). However, the orthogonal normal cross-sections of the channel wall

(in the plane perpendicular to Fig. 1) are not circles except at the crests and the troughs; their curvatures are therefore not evident and should be obtained from the general expressions of differential geometry.

To calculate the principal curvatures of the surface of revolution in Fig. 1, it is convenient to recast it in parametric form using Eq. (A-1).

$$x(u, v) = r_{\max} \left[1 + \frac{1}{2} \left(\frac{r_{\min}}{r_{\max}} \check{S} 1 \right) \left(1 + \cos \pi \frac{u}{L} \right) \right] \cos v, \quad (\text{A-1a})$$

$$y(u, v) = r_{\max} \left[1 + \frac{1}{2} \left(\frac{r_{\min}}{r_{\max}} \check{S} 1 \right) \left(1 + \cos \pi \frac{u}{L} \right) \right] \sin v, \quad (\text{A-1b})$$

$$z(u, v) = u. \quad (\text{A-1c})$$

The principal curvatures can then be found as the roots of the characteristic equation

$$(L \check{S} kE)(N \check{S} kG) \check{S} (M \check{S} kF)^2 = 0, \quad (\text{A-2})$$

where E , F , G , L , M , and N are the coefficients of the first and second fundamental differential quadratic forms (Korn and Korn 1968 Eqs. 17.3D22). Using Eq. A-1, these coefficients can be calculated as follows (Korn and Korn 1968 formulae 17.3D9 and 17.3D19):

$$E(u, v) = \left(\frac{\partial x}{\partial u} \right)^2 + \left(\frac{\partial y}{\partial u} \right)^2 + \left(\frac{\partial z}{\partial u} \right)^2 = 1 + \frac{\pi^2 r_{\max}^2}{4L^2} \left(\frac{r_{\min}}{r_{\max}} \check{S} 1 \right)^2 \sin^2 \pi \frac{u}{L}, \quad (\text{A-3a})$$

$$F(u, v) = \frac{\partial x}{\partial u} \frac{\partial x}{\partial v} + \frac{\partial y}{\partial u} \frac{\partial y}{\partial v} + \frac{\partial z}{\partial u} \frac{\partial z}{\partial v} = 0, \quad (\text{A-3b})$$

$$G(u, v) = \left(\frac{\partial x}{\partial v} \right)^2 + \left(\frac{\partial y}{\partial v} \right)^2 + \left(\frac{\partial z}{\partial v} \right)^2 = r_{\max}^2 \left[1 + \frac{1}{2} \left(\frac{r_{\min}}{r_{\max}} \check{S} 1 \right) \left(1 + \cos \pi \frac{u}{L} \right) \right]^2, \quad (\text{A-3c})$$

$$L(u, v) = \frac{1}{EG \check{S} F^2} \begin{vmatrix} \frac{\partial^2 x}{\partial u^2} & \frac{\partial x}{\partial u} & \frac{\partial x}{\partial v} \\ \frac{\partial^2 y}{\partial u^2} & \frac{\partial y}{\partial u} & \frac{\partial y}{\partial v} \\ \frac{\partial^2 z}{\partial u^2} & \frac{\partial z}{\partial u} & \frac{\partial z}{\partial v} \end{vmatrix} = \frac{\frac{\pi^2 r_{\max}^2}{2L^2} \left(\frac{r_{\min}}{r_{\max}} \check{S} 1 \right) \left[1 + \frac{1}{2} \left(\frac{r_{\min}}{r_{\max}} \check{S} 1 \right) \left(1 + \cos \pi \frac{u}{L} \right) \right] \cos \pi \frac{u}{L}}{EG}, \quad (\text{A-3d})$$

$$M(u, v) = \frac{1}{EG \check{S} F^2} \begin{vmatrix} \frac{\partial^2 x}{\partial u \partial v} & \frac{\partial x}{\partial u} & \frac{\partial x}{\partial v} \\ \frac{\partial^2 y}{\partial u \partial v} & \frac{\partial y}{\partial u} & \frac{\partial y}{\partial v} \\ \frac{\partial^2 z}{\partial u \partial v} & \frac{\partial z}{\partial u} & \frac{\partial z}{\partial v} \end{vmatrix} = 0, \quad (\text{A-3e})$$

$$N(u, v) = \frac{1}{EG \check{S} F^2} \begin{vmatrix} \frac{\partial^2 x}{\partial v^2} & \frac{\partial x}{\partial v} & \frac{\partial x}{\partial u} \\ \frac{\partial^2 y}{\partial v^2} & \frac{\partial y}{\partial v} & \frac{\partial y}{\partial u} \\ \frac{\partial^2 z}{\partial v^2} & \frac{\partial z}{\partial v} & \frac{\partial z}{\partial u} \end{vmatrix}$$

Fig. A-1 Radius of curvature
 $OA = 1/k_2$

$$= \frac{r_{\max}^2 \left[1 + \frac{1}{2} \left(\frac{r_{\min}}{r_{\max}} \right) \left(1 + \cos \pi \frac{u}{L} \right) \right]^2}{EG} = \frac{G}{EG} = \sqrt{\frac{G}{E}}. \quad (\text{A-3f})$$

Because $F(u, v) = 0$ and $M(u, v) = 0$, the characteristic equation simplifies to $(L \pm kE)(N \pm kG) = 0$, from which the roots are $k_1 = L/E$ and $k_2 = N/G$.

Let us first consider the root k_2 . To find its specific expression, it is useful to calculate the derivative of Eq1,

$$r(z) = \frac{\pi r_{\max}}{2L} \left(1 \pm \frac{r_{\min}}{r_{\max}} \right) \sin \pi \frac{z}{L}, \quad (\text{A-4})$$

and notice that $E(u, v) = 1 + r^2(z)$ and $G(u, v) = r^2(z)$, where $r(z)$ is defined by Eq. We thus obtain

$$k_2(z) = \frac{N}{G} = \frac{\overline{G/E}}{G} = \frac{1}{GE} = \frac{1}{r(z)\sqrt{1 + r^2(z)}}. \quad (\text{A-5})$$

From Fig. A-1, it is seen that, since $OA = r(z)$, the quantity in the denominator of (A-5) is the radius OA of the sphere with the center on the z -axis, inscribed in the channel and tangent to the wall at point A (see Fig. A-1). OA is therefore the radius of curvature. Due to axial symmetry, we conclude that k_2 represents the curvature of the normal section at point A perpendicular to the plane of Fig. 1. At the crests and troughs, it naturally reduces to $k_{2\max}$ and $k_{2\min}$, respectively. The second (orthogonal) normal section therefore coincides with the sinusoidal profile in Fig. A-1. Its curvature k_1 can be directly calculated from Eq2 without even resorting to the general Eq2:

$$k_1(z) = \frac{r}{(1 + r^2)^{3/2}} = \frac{\frac{\pi^2 r_{\max}}{2L^2} \left(1 \pm \frac{r_{\min}}{r_{\max}} \right) \cos \pi \frac{z}{L}}{(1 + r^2)^{3/2}}, \quad (\text{A-6})$$

where $r(z)$ is defined in Eq. A-4.

The sum of the principal curvatures to be used in the capillary-pressure calculation in Eq.2 becomes

$$k_2(z) + k_1(z) = \frac{1}{\sqrt{1 + r'^2(z)}} \left[\frac{1}{r(z)} \dot{\S} \frac{\frac{\pi^2 r_{\max}^2}{2L^2} \left(1 \dot{\S} \frac{r_{\min}}{r_{\max}}\right) \cos \pi \frac{z}{L}}{1 + r'^2(z)} \right], \quad (\text{A-7})$$

where the sign of the second term is chosen in such a way that the term is positive under the convex surface, correctly leading to an increase in the capillary-pressure.

Note that the same expression, with the signs appropriately chosen, was used without derivation by Gauglitz and Radkó (1988 Eq. 4) (in dimensionless form) and by Thornton and Homsy (1976 p. 76) with the derivation based on less transparent tensorial formalism. We have provided the derivation that could be easily reproduced (see, for example, Eqs. 12-13) for any parametrically defined surface.

Appendix B: More Accurate Analysis: Capillary-Pressure Distribution Along the Channel

Full Expression for the Capillary Pressure and Locations of the Intermediate Extrema

Using (A-7) in Eq.2, we obtain a continuous distribution of the capillary-pressure along the channel,

$$P_{ca}(z) = \frac{\sigma}{\sqrt{1 + r'^2(z)}} \left[\frac{1}{r(z)} \dot{\S} \frac{\frac{\pi^2 r_{\max}^2}{2L^2} \left(1 \dot{\S} \frac{r_{\min}}{r_{\max}}\right) \cos \pi \frac{z}{L}}{1 + r'^2(z)} \right]. \quad (\text{B-1})$$

By taking the derivative of Eq.1 and equating it to zero, the locations of all extrema in the capillary-pressure can be found. Taking into account (A-4) and omitting the intervening straightforward but tedious algebra, the derivative of (B-1) can be represented as a product of two terms $\Phi_1(z)$ and $\Phi_2(z)$, leading to two decoupled equations,

$$\Phi_1(z) \quad \sin \pi \frac{z}{L} = 0, \quad (\text{B-2})$$

$$\begin{aligned} \Phi_2(z) \quad & \frac{\pi^4 r_{\max}^4 r_{\min}}{8L^4 r_{\max}} \left(2 \dot{\S} \frac{r_{\min}}{r_{\max}}\right) \left(1 \dot{\S} \frac{r_{\min}}{r_{\max}}\right)^2 \cos^4 \pi \frac{z}{L} \\ & \dot{\S} \frac{3\pi^4 r_{\max}^4}{16L^4} \left(1 + \frac{r_{\min}}{r_{\max}}\right) \left(1 \dot{\S} \frac{r_{\min}}{r_{\max}}\right)^3 \cos^3 \pi \frac{z}{L} \\ & + \frac{\pi^2 r_{\max}^2}{L^2} \left(1 \dot{\S} \frac{r_{\min}}{r_{\max}}\right)^2 \left[1 + \frac{\pi^2 r_{\max} r_{\min}}{2L^2} + \frac{3\pi^2 r_{\max}^2}{8L^2} \left(1 \dot{\S} \frac{r_{\min}}{r_{\max}}\right)^2 \right] \cos^2 \pi \frac{z}{L} \\ & \dot{\S} \frac{3\pi^2 r_{\max}^2}{4L^2} \left(1 \dot{\S} \frac{r_{\min}}{r_{\max}}\right) \left(1 + \frac{r_{\min}}{r_{\max}}\right) \left[1 + \frac{\pi^2 r_{\max}^2}{4L^2} \left(1 \dot{\S} \frac{r_{\min}}{r_{\max}}\right)^2 \right] \cos \pi \frac{z}{L} \\ & \dot{\S} \left(1 \dot{\S} \frac{\pi^2 r_{\min} r_{\max}}{L^2}\right) \left[1 + \frac{\pi^2 r_{\max}^2}{4L^2} \left(1 \dot{\S} \frac{r_{\min}}{r_{\max}}\right)^2 \right] = 0. \end{aligned} \quad (\text{B-3})$$

Equation B-2 has roots at $z/L = \pm 0, 1, 2, \dots$, corresponding to the crests and the troughs of the profile (Fig1). These locations contain the extrema of the capillary-pressure, which

was intuitively clear in the derivation of criterion (6) (but has now been proved). On the other hand, the capillary-pressure may also have additional extrema at intermediate points determined by the real roots of the quartic equation (3). Solving such an equation would be a formidable and perhaps unnecessary task. For a wide range of parameter combinations, one can ascertain the character of the solutions and the values of the capillary-pressure at them by means of an approximate analysis.

First, if r_{\min} and r_{\max} are close enough that their ratio is near unity, Eq. (3) reduces to

$$1 - \frac{\pi^2 r_{\min} r_{\max}}{L^2} = 0.$$

If we exclude the particular combination in which $r_{\min} r_{\max} = L^2$ (corresponding to constant p_{ca} along the channel), this equation is never satisfied, meaning that there are no intermediate extrema in the capillary-pressure.

Second, Eq. (3) also significantly simplifies if $r_{\min} \ll r_{\max}$. It is then re-written as

$$\begin{aligned} & \frac{3\pi^4 r_{\max}^4}{16L^4} \cos^3 \pi \frac{z}{L} + \frac{\pi^2 r_{\max}^2}{L^2} \left(1 + \frac{3\pi^2 r_{\max}^2}{8L^2}\right) \cos^2 \pi \frac{z}{L} \\ & - \frac{3\pi^2 r_{\max}^2}{4L^2} \left(1 + \frac{\pi^2 r_{\max}^2}{4L^2}\right) \cos \pi \frac{z}{L} - \left(1 - \frac{\pi^2 r_{\max}^2 r_{\min}}{L^2 r_{\max}}\right) \left(1 + \frac{\pi^2 r_{\max}^2}{4L^2}\right) = 0, \end{aligned} \quad (\text{B-4})$$

which can further be reduced if we notice that coefficients are about the same before $\cos \pi(z/L)$ and $\cos^2 \pi(z/L)$ and consequently neglect the quadratic term,

$$\begin{aligned} & \frac{3\pi^4 r_{\max}^4}{16L^4} \cos^3 \pi \frac{z}{L} - \frac{3\pi^2 r_{\max}^2}{4L^2} \left(1 + \frac{\pi^2 r_{\max}^2}{4L^2}\right) \cos \pi \frac{z}{L} \\ & - \left(1 - \frac{\pi^2 r_{\max}^2 r_{\min}}{L^2 r_{\max}}\right) \left(1 + \frac{\pi^2 r_{\max}^2}{4L^2}\right) = 0. \end{aligned} \quad (\text{B-5})$$

Here, we can still distinguish three useful cases: $r_{\max} \ll L$, $r_{\max} \approx L$, and $r_{\max} \gg L$. The simplest to analyze is $r_{\max} \ll L$, as in this case Eq. (5) reduces to $\tilde{c} = 0$ and is never satisfied. No intermediate extrema exist therefore for the combinations $\{r_{\min} \ll r_{\max}, r_{\max} \ll L\}$ (the braces indicate the simultaneous conditions). In the case $r_{\max} \gg L$, Eq. (5) becomes

$$\frac{3\pi^4 r_{\max}^4}{16L^4} \left(\cos^3 \pi \frac{z}{L} + \cos \pi \frac{z}{L}\right) - \frac{\pi^2 r_{\max}^2}{4L^2} \left(1 - \frac{\pi^2 r_{\max}^2 r_{\min}}{L^2 r_{\max}}\right) = 0, \quad (\text{B-6})$$

which, if we again neglect the higher power of cosine, transforms to

$$\frac{3\pi^2 r_{\max}^2}{4L^2} \cos \pi \frac{z}{L} + \left(1 - \frac{\pi^2 r_{\max}^2 r_{\min}}{L^2 r_{\max}}\right) = 0. \quad (\text{B-7})$$

The roots of Eq. (7) describing the coordinates of the intermediate extrema are

$$\cos \pi \frac{z}{L} = \frac{\pi^2 r_{\max}^2 r_{\min}}{L^2 r_{\max}} - 1, \quad \{r_{\min} \ll r_{\max}, r_{\max} \gg L\}. \quad (\text{B-8})$$

Finally, if $r_{\max} \ll L$, we can re-cast the left-hand side of Eq. 5 approximately as

$$\begin{aligned} & \left[\frac{3\pi^4 r_{\max}^4}{16L^4} \cos^3 \pi \frac{z}{L} \left(1 + \frac{\pi^2 r_{\max}^2}{4L^2} \right) \left(\frac{3\pi^2 r_{\max}^2}{4L^2} \cos \pi \frac{z}{L} + 1 \right) \right. \\ & \left. - \frac{3\pi^4 r_{\max}^4}{16L^4} \cos^3 \pi \frac{z}{L} \left(\frac{\pi^2 r_{\max}^2}{4L^2} \left(\frac{3\pi^2 r_{\max}^2}{4L^2} \cos \pi \frac{z}{L} + 1 \right) \right) \right] \\ & = \frac{3\pi^2 r_{\max}^2}{4L^2} \left(\cos^3 \pi \frac{z}{L} + \cos \pi \frac{z}{L} \right) \approx 1, \end{aligned} \quad (B-9)$$

which, with the same degree of approximation, transforms Eq. 5 to

$$\frac{3\pi^2 r_{\max}^2}{4L^2} \cos \pi \frac{z}{L} + 1 = 0. \quad (B-10)$$

The roots of Eq. 10 describing the coordinates of the intermediate extrema are

$$\cos \pi \frac{z}{L} = -\frac{1}{\frac{3\pi^2 r_{\max}^2}{4L^2}}, \quad \{r_{\min} \ll r_{\max}, r_{\max} \ll L\}. \quad (B-11)$$

Note that Eq. 11 can be obtained from Eq. 8 by setting $r_{\max} \ll L$ in the latter. We therefore can combine them in one approximate equation for the intermediate extrema,

$$\cos \pi \frac{z}{L} = \frac{\frac{\pi^2 r_{\max}^2}{L^2} \frac{r_{\min}}{r_{\max}}}{\frac{3\pi^2 r_{\max}^2}{4L^2}} \approx 1, \quad \{r_{\min} \ll r_{\max}, r_{\max} \gg L \text{ or } r_{\max} \ll L\}. \quad (B-12)$$

Capillary Pressure at the Intermediate Extrema

As we have found out, there are no extrema in the capillary-pressure profile along the channel except those at the troughs and the crests in the cases of $r_{\max} \ll L$ and $r_{\min} \ll r_{\max}, r_{\max} \ll L$. These are the cases of a smoothly varying profile. There are, however, intermediate extrema at least at locations defined by Eq. 11 for $\{r_{\min} \ll r_{\max}, r_{\max} \gg L \text{ or } r_{\max} \ll L\}$. The capillary-pressure at these extrema should be compared to that at the troughs and crests to see if the former may dominate the flow.

For the case of $r_{\min} \ll r_{\max}$ under consideration, the exact expression (Eq. 1) for the capillary-pressure can be simplified similar to the transition from Eq. 3 to (B-4). Then the result can further be reduced, as previously, if we neglect $\cos(z/L)$ compared to unity. Omitting the intervening algebra, we arrive at

$$P_{ca}(z) = \frac{2\sigma \cos \pi \frac{z}{L}}{r_{\max} \sqrt{1 + \frac{\pi^2 r_{\max}^2}{4L^2}}} \left[\frac{1}{\left(1 - \frac{\pi^2 r_{\max}^2}{4L^2} \cos^2 \pi \frac{z}{L} \right) \cos \pi \frac{z}{L}} - \frac{\frac{\pi^2 r_{\max}^2}{4L^2}}{1 + \frac{\pi^2 r_{\max}^2}{4L^2}} \right]. \quad (B-13)$$

Considering that $r_{\max} \gg L$ or $r_{\max} \ll L$, the latter expression is approximately

$$P_{ca}(z) = \frac{2\sigma \cos \pi \frac{z}{L}}{r_{\max}} \left[\frac{1}{\left(1 - \frac{\pi^2 r_{\max}^2}{4L^2} \cos^2 \pi \frac{z}{L} \right) \cos \pi \frac{z}{L}} - 1 \right] - \frac{2\sigma}{r_{\max}} \left(1 - \frac{\pi^2 r_{\max}^2}{4L^2} \cos^2 \pi \frac{z}{L} \right), \quad (B-14)$$

where we still have neglected $\cos^2(z/L)$ compared to $\cos(z/L)$, keeping the same approximation as before. Equation 14 is the approximate expression for P_{ca} for the case in which

Eq.B-12 is valid. Upon substituting Eq. (B-12) into (B-14), the capillary-pressure at the intermediate extrema is obtained as

$$P_{ca}(z) = \frac{2\sigma}{r_{max}} \left(1 \check{\text{S}} \frac{\frac{\pi^2 r_{max}^2 r_{min}}{L^2} \check{\text{S}} 1}{\frac{3\pi^2 r_{max}^2}{4L^2}} \right). \quad (\text{B-15})$$

Further, for the $r_{min} \ll r_{max}$ case of interest, the capillary-pressure at the troughs simplifies to

$$P_{ca}^{trough} = \frac{\sigma}{r_{max}} \left(\frac{r_{max}}{r_{min}} \check{\text{S}} \frac{\pi^2 r_{max}^2}{2L^2} \right). \quad (\text{B-16})$$

Under the same condition, the capillary-pressure at the crests equals

$$P_{ca}^{crest} = \sigma \left(\frac{1}{r_{max}} + \frac{\pi^2 r_{max}}{2L^2} \right) = \frac{\sigma}{r_{max}} \left(1 + \frac{\pi^2 r_{max}^2}{2L^2} \right),$$

which, again considering that $r_{max} \gg L$ or $r_{max} \gg L$, approximately becomes

$$P_{ca}^{crest} = \frac{\sigma \pi^2 r_{max}}{2L^2}. \quad (\text{B-17})$$

We can now estimate the values of the pressure at the intermediate extrema relative to that in the troughs and crests (B-16 and B-17).

For example, let us first take the ratio of Eqs. B-16 to B-15,

$$\frac{P_{ca}^{trough}}{P_{ca}^{interm}} = \frac{\frac{r_{max}}{r_{min}} \check{\text{S}} \frac{\pi^2 r_{max}^2}{2L^2}}{2 \left(1 \check{\text{S}} \frac{\frac{\pi^2 r_{max}^2 r_{min}}{L^2} \check{\text{S}} 1}{\frac{3\pi^2 r_{max}^2}{4L^2}} \right)} = \frac{\pi^2 \left(\frac{2L^2}{\pi^2 r_{max}^2} \check{\text{S}} \frac{r_{min}}{r_{max}} \right)}{4 \frac{r_{min}}{r_{max}} \frac{L^2}{r_{max}^2} \left(1 \check{\text{S}} \frac{4}{3} \frac{r_{min}}{r_{max}} + \frac{4L^2}{3\pi^2 r_{max}^2} \right)}, \quad (\text{B-18})$$

which, again using the conditions $r_{min} \ll r_{max}$, $r_{max} \gg L$ or $r_{max} \gg L$, is approximately

$$\frac{P_{ca}^{trough}}{P_{ca}^{interm}} = \frac{\frac{2L^2}{r_{max}^2} \check{\text{S}} \pi^2 \frac{r_{min}}{r_{max}}}{4 \frac{r_{min}}{r_{max}} \frac{L^2}{r_{max}^2}}. \quad (\text{B-19})$$

This ratio can only be zero if $r_{min} r_{max} = 2L^2$. If we exclude this specific case, two scenarios are possible. At $r_{min} \ll r_{max}$, $r_{max} \gg L$, we have

$$\frac{P_{ca}^{trough}}{P_{ca}^{interm}} \approx \frac{\frac{2L^2}{r_{max}^2}}{4 \frac{r_{min}}{r_{max}} \frac{L^2}{r_{max}^2}} = \frac{1}{2 \frac{r_{min}}{r_{max}}} \gg 1.$$

At $\{r_{min} \ll r_{max}, r_{max} \gg L\}$, we have

$$\frac{P_{ca}^{trough}}{P_{ca}^{interm}} \check{\text{S}} \frac{\pi^2 r_{min}}{4 \frac{r_{min}}{r_{max}} \frac{L^2}{r_{max}^2}} = \check{\text{S}} \frac{\pi^2}{4 \frac{L^2}{r_{max}^2}} \ll \check{\text{S}} 1.$$

In all cases except the excluded one, the absolute value of P_{ca}^{trough} is much greater than that of P_{ca}^{interm} , and the effect of the intermediate extrema can be neglected.

Let us now take the ratio of (B-17) to (B-15),

$$\frac{p_{ca}^{crest}}{p_{ca}^{interm}} = \frac{\frac{\pi^2 r_{max}^2}{2L^2}}{2 \left(1 \pm \frac{\frac{\pi^2 r_{max}^2 r_{min}}{L^2}}{\frac{3\pi^2 r_{max}^2}{4L^2}} \right)} = \frac{3\pi^2}{4 \frac{L^2}{r_{max}^2} \left(3 \pm 4 \frac{r_{min}}{r_{max}} + \frac{4L^2}{\pi^2 r_{max}^2} \right)}. \quad (B-20)$$

Under the conditions $r_{min} \ll r_{max}$, $r_{max} \gg L$ or $r_{max} \approx L$, it simplifies to

$$\frac{p_{ca}^{crest}}{p_{ca}^{interm}} = \frac{\pi^2}{4 \frac{L^2}{r_{max}^2}}. \quad (B-21)$$

At $r_{max} \approx L$, $p_{ca}^{crest}/p_{ca}^{interm} > 1$, and at $r_{max} \gg L$, $p_{ca}^{crest}/p_{ca}^{interm} \gg 1$. In neither case the capillary-pressure at the intermediate extrema dominates the flow: it is either of the same order of magnitude than that at the crests or much smaller.

We conclude that, in either of the parameter combinations considered ($r_{max} \approx L$ or $r_{min} \ll r_{max}$) and any L , the intermediate extrema either do not exist or exist but do not control the flow. Condition (6) for the spontaneous break-up of the non-wetting fluid thus remains valid even if the continuous pressure distribution along the fluid is taken into account.

References

- Atherton, R.W., Homsy, G.M.: On the derivation of evolution equations for interfacial waves. *Chem. Eng. Commun.* 2, 57-77 (1976). doi:10.1080/00986447608960448
- Beresnev, I.A.: Theory of vibratory mobilization of nonwetting fluids entrapped in pore constrictions. *Geophysics* 71, N47-DN56 (2006)
- Bretherton, F.P.: The motion of long bubbles in tubes. *J. Fluid Mech.* 166-188 (1961). doi:10.1017/S0022112061000160
- De Gennes, P.-G., Brochard-Wyart, F., Quéré, D.: *Capillarity and Wetting Phenomena*. Springer, Heidelberg (2004)
- Gauglitz, P.A., Radke, C.J.: An extended evolution equation for liquid film breakup in cylindrical capillaries. *Chem. Eng. Sci.* 43, 1457-1465 (1988). doi:10.1016/0009-2509(88)85137-6
- Gauglitz, P.A., Radke, C.J.: The dynamics of liquid film breakup in constricted cylindrical capillaries. *J. Colloid Interface Sci.* 134, 14-40 (1990). doi:10.1016/0021-9797(90)90248-M
- Graustein, W.C.: *Differential Geometry*. Dover, New York (2006)
- Hammond, P.S.: Nonlinear adjustment of a thin annular film of viscous fluid surrounding a thread of another within a circular cylindrical pipe. *J. Fluid Mech.* 137, 363-384 (1983). doi:10.1017/S0022112083002451
- Hemmat, M., Borhan, A.: Buoyancy-driven motion of drops and bubbles in a periodically constricted capillary. *Chem. Eng. Commun.* 148-150, 363-384 (1996). doi:10.1080/00986449608936525
- Korn, G.A., Korn, T.K.: *Mathematical Handbook for Scientists and Engineers*, 2nd edn. McGraw-Hill, New York (1968)
- Kovscek, A.R., Tang, G.-Q., Radke, C.J.: Verification of Roof snap off as a foam-generation mechanism in porous media at steady state. *Colloids Surf. A Physicochem. Eng. Appl.* 205, 251-260 (2007). doi:10.1016/j.colsurfa.2007.02.035
- Lamb, H.: *Hydrodynamics*, 6th edn. Cambridge University Press, Cambridge (1997)
- Martinez, M.J., Udell, K.S.: Axisymmetric creeping motion of drops through a periodically constricted tube. In: Wang, T.G. (ed.) *Drops and Bubbles*, AIP Conference Proceedings 197, pp. 222-234. American Institute of Physics, New York (1989)
- Melrose, J.C., Brandner, C.F.: Role of capillary forces in determining microscopic displacement efficiency for oil recovery by water flooding. *J. Can. Pet. Technol.* October-December, 54-62 (1974)
- Middleman, S.: *Modeling Axisymmetric Flows*. Academic Press, New York (1995)
- Olbricht, W.L., Leal, L.G.: The creeping motion of immiscible drops through a converging/diverging tube. *J. Fluid Mech.* 134, 329-355 (1983). doi:10.1017/S0022112083003390
- Roof, J.G.: Snap-off of oil droplets in water-wet pores. *Soc. Pet. Eng. J.* 10, 35-90 (1970). doi:10.2118/2504-PA

- Rossen, W.R.: A critical review of Roof snap-off as a mechanism of steady-state foam generation in homogeneous porous media. *Colloids Surf. A Physicochem. Eng.* **225**, 1924 (2003). doi10.1016/S0927-7757(03)00309-1
- Tsai, T.M., Miksis, M.J.: Dynamics of a drop in a constricted capillary tube. *J. Fluid Mech.* **197**, 217 (1994). doi10.1017/S0022112094002090